Enhanced mitochondrial biogenesis promotes cell survival in human stem cell derived retinal ganglion cells of the central nervous system

Michelle Surma[1,6], Kavitha Anbarasu[1,2,6], Kang-Chieh Huang[3], Jason S. Meyer[1,2,3,4] and Arupratan Das[1,2,4,5,*]

[1]Department of Ophthalmology, Eugene and Marilyn Glick Eye Institute, Indiana University, Indianapolis, IN 46202, USA; [2]Department of Medical and Molecular Genetics, Indiana University, Indianapolis, IN 46202, USA; [3]Department of Biology, Indiana University Purdue University Indianapolis; [4]Stark Neurosciences Research Institute, Indiana University, Indianapolis, IN 46202, USA

[5]Lead Contact

[*]Correspondence: arupdas@iu.edu

[6]These authors contributed equally: Michelle Surma, Kavitha Anbarasu

Mitochondrial dysfunction has been the primary suspect for central nervous system (CNS) disorders such as glaucoma, Parkinson's disease (PD) and amyotrophic lateral sclerosis (ALS). It is still unclear the fundamental mitochondrial quality control (MQC) step that could be improved for developing CNS neuroprotection. Here, we used human stem cell differentiated retinal ganglion cells (hRGCs) of CNS which are the neurons most sensitive towards mitochondrial dysfunction, to identify mechanism of improving MQC. We found hRGCs are highly efficient in promoting mitochondrial biogenesis, a critical step of MQC to compensate for the loss of damaged mitochondria. Pharmacological activation of the cellular energy sensor AMPK resulted in increased mitochondrial biogenesis and energy homeostasis as revealed by biochemical, imaging, metabolic and ultrastructure analysis. This led to enhanced cell survival for both the wild-type and glaucomatous (*OPTN-E50K*) hRGCs providing a foundation for developing neuroprotection for broad range of optic neuropathies and CNS disorders irrespective of genetic mutations.

Introduction

Neurons require a steady supply of ATP compared to other cells to establish membrane potential for neurotransmission and synaptic activity[1]. Oxidative phosphorylation in mitochondria is the primary source of cellular ATP, thus mitochondrial dysfunction often associates with the neurodegenerative diseases such as mitochondrial optic neuropathies (MONs)[2], Parkinson's disease (PD)[3] and amyotrophic lateral sclerosis (ALS)[4]. Among central nervous system (CNS) neurons, retinal ganglion cells (RGCs) of the optic nerve are the most sensitive towards mitochondrial dysfunction. As such, inherited mutations in the complex I subunit of respiratory chain cause Leber's hereditary optic neuropathy (LHON)[5], OPA1 mutations of the mitochondrial outer membrane protein required for mitochondrial fusion cause dominant optic atrophy (DOA)[6], together known as MONs. Similarly, other mutations have been found in the mitochondrial quality (MQC) pathways are associated with the normal-tension glaucoma (NTG)[7]. Intriguingly, these inherited mitochondrial mutations, though present in every cell of a patient's body, only cause RGC death leading to optic neuropathies. Thus, RGCs serve a great neuronal model of the CNS for investigating mechanism of improving mitochondrial homeostasis for developing neuroprotection. MQC involves biogenesis of healthy mitochondria, fusion, fission and degradation of damaged mitochondria (mitophagy). The most common MQC mutation found among NTG patients (~17% prevalence) is a missense mutation in the mitophagy gene Optineurin (OPTN-E50K, E50K here on)[8,9]. Thus, reduced mitochondrial homeostasis is expected in the E50K RGCs. However, to date we have very limited understanding on how to improve MQC for developing neuroprotection associated with aging and genetic disorders.

AMP-activated protein kinase (AMPK) is the master energy sensor in cells and a decline in energy homeostasis associates with aging[10], obesity[11] and neurodegeneration[12]. Healthy mitochondria are the key source of cellular energy; thus it is expected decline in mitochondrial homeostasis could lead to energy stress in above disease conditions. Energy stress activates AMPK which activates proliferator-activated receptor gamma co-activator 1α (PGC-1α)[13] which is the master regulator of mitochondrial biogenesis.

Under normal condition, TBK1 phosphorylates the inhibitory site of AMPK[14] limiting energy expenditure which becomes counterproductive during aging and obesity. Conversely, TBK1 inhibition has been found to increase energy expenditure, reduce obesity and insulin resistance in mice[11]. It has not been studied if activating mitochondrial biogenesis and targeting TBK1 could improve energy homeostasis in CNS neurons ultimately leading to neuroprotection.

Here, we used a well characterized robust human stem cell differentiated RGC (hRGC) model to investigate if improving energy homeostasis through TBK1-AMPK pathway could promote MQC and neuroprotection. It is critical to investigate the MQC mechanisms in human RGCs as mice RGCs are intrinsically very different from human[15]. Differentiated hRGCs used here show the hallmark of human RGCs, as characterized by their morphological features, gene-expression pattern, and electrophysiological properties such as spontaneous generation of action potentials[16,17] and ability to graft in the mice retina[18]. We have shown here that hRGCs activate mitochondrial biogenesis pathway in response to mitochondrial damage to maintain mitochondrial homeostasis. Furthermore, TBK1 inhibition activated the AMPK-PGC-1α biogenesis axis and mitochondrial mass in hRGCs. Remarkably, activation of mitochondrial biogenesis increased cell survival and energy homeostasis through increased respiratory capacity for both the wild-type and glaucomatous E50K hRGCs as an indication for neuroprotection.

Results

RGCs produce healthy mitochondria to maintain homeostasis under stress. To investigate mitochondrial homeostasis mechanism in human RGCs we have used human stem cell differentiated RGCs (hRGCs) following a robust method[16,19] where cells express RGC specific marker RBPMS and neuronal marker Tubulin β3 (**Supplementary Fig. 1a, b**). We have developed "disease in a dish" model for glaucoma using CRISPR engineered human embryonic stem cells (H7-ESCs-E50K) (**Supplementary Fig. 1c**), patient derived induced pluripotent stem cells with the mutation (iPSCs-E50K)[20] and corresponding H7-ESC and iPSC-E50K corrected (iPSC-E50Kcorr)[21] reporter lines for isogenic controls. RGCs are

among the most metabolically demanding CNS neurons due to their steady need for ATP for spontaneous action potential firing[22]. As mitochondria are the primary source for cellular ATP, it is likely that RGCs will be highly sensitive towards mitochondrial damage. However, we had shown even after 24h of treatment with a potent mitochondrial stressor CCCP, hRGCs degrade damaged mitochondria with minimal cell death[19]. This suggests the existence of a compensatory pathway for the loss of mitochondria or hRGCs are well-tolerated for mitochondrial loss. Here, we tested whether hRGCs maintain the same total mitochondrial mass during the CCCP damage by western blot (WB) against the mitochondria specific protein Tom70. Interestingly, we found total mitochondrial mass for both the WT and E50K-hRGCs remained similar to the DMSO control condition (**Fig. 1a, b, c)** which was further validated by the confocal immunofluorescence (IF) imaging of mitochondria specific Tom20 protein (**Fig. 1d, e**). Of note, CCCP treatment caused mitochondrial network more fragmented (**Fig. 1d**). There was moderate loss of total mitochondrial mass as an early response to CCCP for both WT (1h) and E50K (6h) hRGCs while cells regained mitochondrial mass similar to the control condition at the longer treatment (24h) (**Fig. 1e**). While hRGCs maintained total mitochondrial mass under acute mitochondrial damage, it is possible to have a positive-feedback where cells degrade damaged mitochondria which activates the biogenesis pathway to compensate the loss. To directly measure if CCCP damage induces mitochondrial degradation, first we have labelled hRGCs with mitochondria specific live cell dye, MitoTracker Deep Red (MTDR) followed by CCCP treatment and mitochondrial mass measurement over time by flowcytometry in the absence of MTDR dye in the media as developed by us[19]. This experimental design allows only to monitor the labelled mitochondrial population under CCCP damage but not the newly synthesized population. Flow cytometry gating strategy is explained in **Supplementary Fig. 2**. Quite interestingly, we observed robust mitochondrial degradation for both the WT and E50K-hRGCs (**Fig. 1f**). Since total mitochondrial mass remained similar with CCCP treatment (**Fig. 1a-e**), we asked if mitochondrial loss is compensated by the biogenesis of new mitochondria. To directly measure the mitochondrial biogenesis step, we have modified the flow experimental design, where we first labelled hRGCs with MTDR along with CCCP treatment for

3h to cause mitochondrial degradation. We then washed CCCP off with media containing only MTDR and monitor MTDR labelled mitochondrial mass over time. In this design, we will be able to identify the loss of mitochondrial population after 3h CCCP treatment in comparison to DMSO control and then monitor increase in mitochondrial mass in the absence of CCCP. Indeed, we observed severe loss of mitochondria immediately after CCCP treatment, but the mass gradually increased over time and became similar to the DMSO control after 24h of wash (**Fig. 1g**). These suggest hRGCs maintain mitochondrial homeostasis through biogenesis under mitochondrial stress.

To visualize the biogenesis event, we used live cell JC1 dye which fluoresces green (monomers) when bound to damaged and red (J aggregates) when bound to healthy mitochondria[23]. We labelled mitochondria with the JC1 dye and then added CCCP in presence of the dye to monitor damaged and newly synthesized populations. Interestingly, we observed an increase in JC1 red (**Fig. 2a, c, d)** but more fragmented network and decrease in JC1 green mitochondria (**Fig. 2a, b, d)** for both the WT and E50K-hRGCs upon CCCP damage. This suggests hRGCs are producing more mitochondria under damage which presumably getting damaged and fragmented as we have CCCP stressor in the imaging media. Interestingly, E50K-hRGCs showed higher red mitochondria compared to the WT both before and after CCCP treatments (**Fig. 2c**) and moderate increase in green (damaged) mitochondria before CCCP damage (**Fig. 2b**). This suggests E50K-hRGCs possess damaged mitochondria under basal conditions which trigger biogenesis as detected by increase in JC1 red fluorescence while decrease in green fluorescence under CCCP reflects mitophagy of damaged mitochondria.

hRGCs activate biogenesis signaling pathway under mitochondrial damage. Mitochondrial biogenesis has been shown to induce muscle growth after exercise[24] and synaptic plasticity in neurons[25]. However, it is unknown if mitochondrial damage triggers activation of biogenesis pathway in CNS neurons and how to leverage the biogenesis pathway for developing neuroprotection. PGC-1α is the master regulator of mitochondrial biogenesis[26] which is a transcriptional co-activator of nuclear respiratory factor 2 (NRF2) and NRF1 which activates transcription factor A, mitochondrial (TFAM) for mitochondrial DNA

(mtDNA) gene expressions[27]. The biogenesis pathway can also be activated by the transcriptional co-activators PGC-1β and PGC1 related co-activator (PRC)[28]. We induced mitochondrial damage in hRGCs and measured biogenesis pathway gene expressions such as PGC-1α, PGC-1β, NRF2, NRF1 and PRC. Indeed, we observed increase of these gene expressions in the WT and E50K hRGCs upon CCCP mediated mitochondrial damage (**Fig. 3a-d**). At the protein level, both WT and E50K hRGCs showed increased PGC-1α with prolonged mitochondrial damage (24h, CCCP), however E50K showed slower increase at earlier time points (**Fig. 3e, f**).

AMP-activated protein kinase (AMPK) is a key regulator of energy sensing and responds by increasing mitochondrial biogenesis[29]. AMPK is a heterotrimeric protein activated by the phosphorylation of Thr172 in the AMPKα subunit[30] which in turn activates PGC-1α[11]. We asked if mitochondrial damage leads to reduced energy production and activation of AMPKα for mitochondrial biogenesis in hRGCs. Indeed, under mitochondrial damage both AMPKα protein level (**Fig. 3e, g**) and Thr172 phosphorylation level (**Fig. 3e, h, i**) increased in the WT hRGCs with much less increase for the E50K hRGCs (**Fig. 3e, g, h, i**). This suggests E50K-hRGCs have defective AMPK mediated energy sensing pathway.

E50K hRGCs are defective in TBK1 inhibition mediated AMPK activation. Crystal structure revealed OPTN dimerizes in solution; however, glaucomatous E50K mutation forms tetrameric aggregates[31]. OPTN-E50K mutation forms tight electrostatic interaction with the E698 residue of TBK1 kinase resulting insoluble aggregates[31,32] potentially inhibiting OPTN function. BX795 (BX, here on) drug is a potent TBK1 inhibitor[33] that has been shown to resist the nerve fiber layer thinning of the E50K transgenic mice retina[34]. Conversely, an increased copy number of the TBK1 gene are found in the NTG patients[35,36]. To elucidate, if E50K forms aggregates in the hRGCs, we performed confocal immunofluorescence (IF) imaging and observed increased OPTN aggregates in the E50K-hRGCs which got mostly dissolved by TBK1 inhibition using BX (**Fig. 4a, b**). The mechanisms of BX mediated OPTN-E50K aggregate dissolution will require further studies.

It was also reported that TBK1 inhibits AMPK in adipose tissue, and AMPK activation promotes mitochondrial biogenesis through PGC-1α[11]. Thus, TBK1 inhibition could promote mitochondrial biogenesis in hRGCs. We observed similar level of mitochondrial mass between the DMSO control and BX treatment for both the WT and E50K hRGCs (**Fig. 4a, c, d**). However, at a longer BX treatment, we saw increase in mitochondria mass for the WT (48h, 72h) (**Fig. 4c**) and for E50K (72h) (**Fig. 4d**) hRGCs. To investigate if BX treatment caused initial increase in mitochondrial mass but cells regain homeostasis during longer treatment, we measured mitochondrial mass by western blots against Tom70 protein at early and longer BX treatments. We saw an initial increase in mitochondrial mass as an early response (6h) of TBK1 inhibition by BX which returned to the basal level during prolonged treatment (18h, 24h) for both the WT and E50K hRGCs (**Fig. 4e, f**). Taking tother, these data suggest hRGCs go through cyclic changes of increase and decrease of mitochondrial mass under TBK1 inhibition presumably to maintain cellular energy homeostasis.

To test if TBK1 inhibition activates cellular energy sensing pathway by activating AMPK, we measured Thr172 phosphorylation of the AMPKα subunit. Interestingly, we observed moderate increase in the AMPKα level (**Fig. 4g, h)** for both the WT and E50K hRGCs. However, phospho(Thr172)-AMPKα increased significantly compared to DMSO control in the WT but not in the E50K hRGCs (**Fig. 4g, i)**. These suggest TBK1 inhibition mediated AMPK activation pathway is defective in the E50K hRGCs. However, E50K hRGCs maintained mitochondrial homeostasis under TBK1 inhibition, suggesting AMPK independent regulation of mitochondrial biogenesis.

Mitochondrial ultrastructure reveals TBK1 inhibition increases mitochondrial coverage and quality in hRGCs. To understand the effect of TBK1 inhibition on mitochondrial quality and mass, we initially quantified the mitochondrial levels in the wild-type and mutant cells under basal conditions. Estimation of Tom20 levels using confocal immunofluorescence imaging showed that the total mitochondrial mass in E50K was lower compared to WT hRGCs (**Fig. 5a, b**). Next, to obtain direct evidence if TBK1 inhibition increases mitochondrial mass and quality in hRGCs, we performed

transmission electron microscopy (TEM) and measured mitochondria area and morphology in presence of BX. We observed a lower number of mitochondrial section areas per unit area of cytoplasm (mitochondrial coverage) in glaucomatous E50K hRGCs compared to WT hRGCs, which improved upon BX treatment in both cell types (**Fig. 5c, d).** Mitochondrial swelling has been shown to play a role in several neurodegenerative diseases as it involves ion balance disruption and opening of transition pores, leading to cell death[37]. We assessed if E50K hRGCs have swelled mitochondria and if TBK1 inhibition by BX reduces mitochondrial swelling by measuring perimeter, major and minor axis lengths of the mitochondrial sections. Mitochondrial perimeter was significantly higher in the E50K hRGCs than WT, which was reduced by BX (**Fig. 5e)**. We further observed both the major and minor axis of mitochondria were significantly higher in the E50K hRGCs than WT (**Fig. 5c, f, g**). BX treatment reduced major axis length in the E50K hRGCs (**Fig. 5f)** with moderate reduction for the minor axis length **(Fig. 5g)**. This suggests E50K hRGCs possess swelled mitochondria with reduced mitochondrial coverage and TBK1 inhibition improved both the swelling and coverage as an indication for improved mitochondrial physiology.

TBK1 inhibition promotes energy homeostasis and cell survival in hRGCs. RGCs are progressively degenerating neurons which exacerbates under aging and disease conditions[38]. Our data showed TBK1 inhibition promoted mitochondrial biogenesis and improved morphology in hRGCs. We asked if this treatment improves cellular respiration and viability for both the WT and glaucomatous E50K hRGCs. Using seahorse analyzer, we observed TBK1 inhibition increased oxygen consumption rate (OCR) (**Fig. 6a, b**) and spare respiratory capacity (**Fig. 6c**) for both the WT and E50K hRGCs. An increase in spare respiratory capacity reflects cells' ability to produce additional ATP by oxidative phosphorylation to combat degenerative conditions[39]. Thus, a TBK1 inhibition mediated increase in spare respiratory capacity is the indication for improved energy homeostasis and RGC neuroprotection. To assess the direct effect of TBK1 inhibition on cell survival, we measured hRGC viability and apoptosis by caspase-3/7 activity in presence of BX. Remarkably, we observed BX increased viability for both the WT and E50K hRGCs (**Fig. 6d**) with corresponding reduction of the cellular apoptosis (**Fig. 6e**). For patient derived iPSCs, we observed

minimal effect on cell viability but reduced cellular apoptosis for both the E50K-corrected and E50K hRGCs (**Fig. 6d, e**).

These suggest TBK1 inhibition improves mitochondrial quality leading to improved energy homeostasis and cell survival for both the WT and glaucomatous RGC neurons. As mitochondrial dysfunctions, mutations in OPTN and TBK genes are involved in broad range of CNS neurodegenerative conditions, this study could be applicable for developing neuroprotection strategy for other CNS disorders.

Discussion

In this study, we have identified mitochondrial biogenesis as a critical step of MQC which could be activated to promote cell survival for both the WT and glaucomatous E50K RGCs. RGCs are highly sensitive towards mitochondrial damage as they need a steady source of ATP for spontaneous action potential firing[22]. Mitochondrial damage potentially disrupts ATP supply and triggers an energy sensing pathway through AMPK[29]. We have shown here acute damage to mitochondria activates mitochondrial biogenesis in RGCs with robust clearance of damaged mitochondria to maintain mitochondrial homeostasis and energy supply. Activation of the biogenesis occurs through the AMPK-PGC-1α biogenesis axis. Previously, it was reported, that the mitochondrial biogenesis activation could be pro cell survival as it associates with exercise induced muscle growth[24] and synaptic plasiticity[25]. In support to this notion, we found robust increase of mitochondrial biogenesis in RGCs with minimal cell death under mitochondrial stress as we previously reported[19].

Mitochondrial biogenesis is central to the maintenance of energy homeostasis which is critical for neuronal health. AMPK functions as an energy sensor and responds to energy stress by activating mitochondrial biogenesis[29,40,41]. It has been shown in mice adipose tissue that TBK1 inhibits AMPK activity causing suppression of energy expenditure, obesity and inflammation[11]. TBK1 is also a key effector for cellular inflammation in response to pro-inflammatory stimuli, and TBK1 inhibition led to reduced obesity, inflammation, insulin resistance and more energy expenditure in mice in response to high-fat diet[11]. Thus, TBK1 provides a very attractive target for developing neuroprotection through improving energy

expenditure which remains unexplored for the CNS disorders. We have shown here that TBK1 inhibition leads to the activation of AMPK in the WT but not in the E50K hRGCs. However, it reduced mitochondrial swelling in the E50K hRGCs, presumably that caused improved mitochondrial homeostasis, respiratory capacity and cell survival. This also suggests TBK1 inhibition mediated improvement of mitochondrial physiology is independent of AMPK activation in the E50K hRGCs. It is intriguing to see improved cell survival and respiratory capacity even in the WT hRGCs in response to TBK1 inhibition which may suggest if these neurons are not in the homeostatic condition. However, it is known RGC neurons are spontaneously degenerating neurons with reduced mitochondrial function[38,42]. Thus, findings here become more important particularly for developing RGC protection for optic neuropathies where no obvious genetic disorders are associated, such as during aging and in high intra-ocular pressure induced glaucoma. Of note, TBK1 copy number increase mutations are found among the normal-tension glaucoma patients[35]. This may lead to reduced mitochondrial biogenesis and quality mediated RGC death. Our study provides a therapeutic strategy where TBK1 inhibition could promote mitochondrial homeostasis mediated RGC neuroprotection for above glaucoma conditions.

Conflicting evidence suggest TBK1 inhibition could activate[11,43] or inhibit[44] cellular inflammation and activation of inflammation leads to cell death. As TBK1 inhibition resulted in increased RGC survival, it is unlikely to activate inflammation. TBK1 activity is also critical for activating the mitophagy proteins such as OPTN, NDP52, TAX1BP1 and P62 for successful mitophagy[45] and defects in the mitophagy could lead to neurodegeneration[46]. However, it is also reported that activation of the above mitophagy proteins could occur independent of TBK1 but through ULK1 kinase[47]. Thus, the neuroprotective effect of TBK1 inhibition we report is unlikely to cause mitophagy defects. However, further studies will be required to elucidate the effect of TBK1 inhibition on inflammation and mitophagy processes in RGCs and other CNS neurons. We show TBK1 inhibition reduced mitochondrial swelling and improved cell survival and respiration for E50K hRGCs, further study will require to elucidate the mechanisms of this improvement.

Mitochondrial dysfunction is the root cause for optic neuropathies such as LHON, DOA[2] and some cases of glaucoma[7]. Our study provides a neuroprotection strategy for broad range of optic neuropathies

irrespective of the genetic disorders. Severe mitochondrial abnormality has been reported for dopaminergic neurons[3] and motor neurons[4] in PD and ALS respectively. Our study could be applicable to test if TBK1 inhibition leads to increased mitochondrial homeostasis and neuroprotection for these CNS disorders.

Acknowledgements

We thank the Broxmeyer laboratory and the Hypoxia Core Facility of the Indiana University Cooperative Center for Excellence in Hematology (U54 DK106846) for their helpful discussion and assistance in Seahorse experiments; D. Zack for valuable discussions and H7-hESC reporter line; C. Miller from Electron Microscopy Core for sample processing and TEM imaging; S. Dutta for critical comments and proof reading and G. Eckert for providing consultations on statistical analysis. This project was funded, in part, with support from the Indiana Clinical and Translational Sciences Institute; National Institutes of Health, USA (R00EY028223); The Glaucoma Foundation; by an award from Ralph W. and Grace M. Showalter Research Trust and the Indiana University School of Medicine; and by the Paul and Carole Stark Fellowship along with Grants in aid of research from Sigma Xi - The Scientific Research Honor Society, to the graduate student K. Anbarasu.

Author contributions

A.D. conceived and supervised the project. A.D., M.S., K.A. designed and performed experiments and analyzed data. K.C.H., and J.M. developed the E50K reporter lines and revised the manuscript. M.S., K.A. and A.D wrote the manuscript.

Competing interests

The Authors declare no competing interests.

Additional information

Supplementary information is available online.

Correspondence and requests for materials should be directed to Arupratan Das (arupdas@iu.edu)

Methods

Reagents and resources: All the reagents including qPCR primers, antibodies and software used are listed in the Supplementary table 1

ESC maintenance:

Human embryonic stem cell (H7-hESCs; WiCell, Madison, WI, https://www. wicell.org) reporter line with CRISPR engineered multicistronic BRN3B-P2A-tdTomato-P2A-Thy1.2 construct into the endogenous RGC specific BRN3B locus was used for isogenic control. CRISPR mutated H7-hESC reporter with $OPTN^{E50K\text{-}homozygous}$ mutation (H7-E50K) was done as explained previously[21]. Patient derived induced pluripotent stem cells (iPSCs) with E50K mutation[20] (iPSC-E50K), E50K mutation corrected to WT by CRISPR in the patient derived iPSC (iPSC-E50Kcorr)[21] with BRN3B::tdTomato reporter were obtained from Jason Meyer lab. All the above cell lines were grown in mTeSR1 media (mT) at 37ºC in 5%CO_2 incubator on matrigel (MG) coated plates. These cells were maintained by clump passaging using Gentle Cell Dissociation Reagent (GD) after 70-80% confluency. Media was aspirated and GD was added to cells followed by incubation at 37ºC in 5%CO_2 incubator for 5 minutes. Next, mT was used to break up the colonies into small clumps by repeated pipetting and then seeded onto new MG plates.

hRGC differentiation and immunopurification:

For differentiation, stem cells were dissociated to single cells using accutase for 10 min and then quenched with twice the volume of mT with 5 μM blebbistatin (blebb). The cells were centrifuged at 150g for 6 minutes and resuspended in mT with 5 μM blebb. 100,000 cells were seeded per well of a 24 well MG coated plate. Next day, media was replaced with mT without blebb. After 24 hours, media was replaced

with differentiation media (iNS) and further small molecule-based differentiation was carried out with iNS media as elucidated previously[19]. hRGC differentiation was monitored by tdTomato expression and cells were purified during days 45-55 using THY1.2 microbeads and magnetic activated cell sorting system (MACS, Miltenyi Biotec) as explained before[16,19]. hRGCs were resuspended in iNS media, counted using a hemocytometer and seeded on MG coated plates or coverslips for experiments.

Flow Cytometry

Purified hRGCs were seeded at 30,000 cells per well of a 96well MG coated plate and maintained for 3 days. For measuring mitochondrial mass, hRGCs were labeled with mitochondria specific MTDR dye. To measure mitochondrial degradation, hRGCs were labeled with 10 nM MTDR dye for 1 hour, washed, and then treated with 10 μM CCCP for a timecourse. To measure mitochondrial biogenesis, hRGCS were labeled with MTDR first, then treated with 10 μM CCCP or equal amount of DMSO for 3 hours, then washed and incubated with fresh media with MTDR for the timecourse. After treatments, hRGCs were dissociated to single cell suspension using accutase and analyzed using Attune NxT flow cytometer (Thermo Fisher).

Western Blot:

Purified hRGCs were seeded at 250,000 cells per well of 24 well MG coated plates and maintained for 3 days. The cells were then treated (10μM CCCP, 1μg/ml BX795 or equivalent volume of DMSO) for the designated durations. DMSO used as the control as small molecules were dissolved in DMSO. The cells were lysed and collected in 100 μl of M-PER extraction buffer with 0.5M EDTA and protease inhibitors. Protein quantification was done using a BSA standards following the DC Protein Assay Kit II (Bio-Rad) and microplate reader. Loading samples were prepared with heat denaturation at 95°C for 5 minutes with laemmli sample buffer (1X). 10-20 μg protein per sample were run on Bio-Rad Mini-PROTEAN TGX precast gels in running buffer (Tris-Glycine-SDS buffer; Bio-Rad) at 100V until the dye front reached to the bottom. The transfer sandwich was made using PVDF membrane (activated in methanol) in Tris-

Glycine transfer buffer (Bio-Rad) with 20% methanol and transferred for 2 hours at 30V, 4ºC. For the visualization of proteins, the membranes were blocked in 5% skim milk in TBST (TBS buffer with 20% Tween20) for 2 hours at room temperature and incubated overnight at 4°C in 1:1000 dilution of primary antibodies for Tom70 (Novas Biologicals), PGC 1α (Abcam), PGC 1β (Abcam), AMPKα (Cell Signaling Technologies, CST), Phospho-AMPKα^{Thr172} (CST), GAPDH (CST), or Actin (CST). Membranes were then washed 3 times for 5 minutes each in TBST, followed by 2h incubation in 5% milk in TBST containing anti-rabbit HRP linked secondary antibody (CST) at 1:10,000 dilution. The membrane was again washed 3 times with TBST and then placed in Clarity Max Western ECL (Bio-Rad) substrate for 5 minutes. The membranes were imaged in a Bio-Rad ChemiDoc Gel Imager, and the band intensities were quantified and normalized with respect to the GAPDH or Actin for that sample using image J.

Immunofluorescence and Confocal imaging:

Purified hRGCs were seeded on MG coated coverslips (1.5 thickness) at a density of 30,000 - 40,000 cells per coverslip and grown for 3 days. hRGCs were then treated (10μM CCCP, 1μg/ml Bx 795 or equivalent volume of vehicle control DMSO), for the indicated time points. After treatment, the media was aspirated, the cells were washed with 1X PBS, and then fixed with 4% Paraformaldehyde for 15 min at 37ºC. Fixed cells were permeabilized with 0.5% Triton-X100 in PBS for 5 min and then washed with washing buffer (1% donkey serum, 0.05% Triton-X100 in PBS) 3 times for 5 minutes each. Cells were blocked with blocking buffer (5% donkey serum, 0.2% Triton-X100 in PBS) for 1 hour. After blocking, antibodies against Tom20 (Mouse, Santa Cruz) and Optineurin (Rabbit, Cayman Chemicals) were added (1:200 in blocking buffer) and the coverslips were incubated overnight at 4ºC. Next, washed with washing buffer 3 times for 5 minutes each and incubated for 2 hours at room temperature in the dark with secondary antibodies, donkey anti-mouse Alexa-488 (Invitrogen) and anti-rabbit Alexa-647 (Invitrogen) (1:500). The coverslips were washed with washing buffer 3 times for 5 minutes each, with 1.43 μM DAPI added to the second wash. The coverslips were then mounted onto slides with DAKO. Visualization of mitochondria

and optineurin (OPTN) aggregates was done by confocal immunofluorescence. Z-stacks of cells were taken using Zeiss LSM700 with 63x/1.4 oil objective. Analysis was carried out using ImageJ with maximum projections of DAPI channel (number of nuclei) and sum projections of TOM20 and OPTN channels. For OPTN aggregate size, we analyzed particles from 0.02 a.u. to infinity.

qPCR:

Purified hRGCs were seeded at 300,000 cells per well of 24 well MG coated plates and maintained for 3 days. Cells were then treated (10μM CCCP, 1μg/ml Bx 795 or equivalent volume of DMSO) for the designated durations. Media was aspirated and cells were incubated in 200 μl Accutase for 10 min and then quenched with 400 μl iNS media. Cells were centrifuged at 150G for 6 min, media aspirated, and the cell pellets were stored at -20°C. RNA was extracted from cell pellets following the kit protocol (Qiagen 74104). The RNA concentration was measured using Nanodrop 2000c (Thermo) and 6 μl of RNA was used to prepare cDNA following the kit protocol (Abm #G492). qPCR primers were designed as detailed in Table S1. qPCR was performed using BlasTaq qPCR MasterMix with 100 ng total cDNA in a 20 μl reaction mixture using QuantStudio6 Flex RT PCR system (Applied Biosystems). GAPDH or actin was used as a housekeeping gene in every plate to calculate the ΔCt values. The ΔΔCt was calculated with respect to the average ΔCt of the control sample. All conditions were measured by averaging 3 technical repeats for each biological repeat with total 3 biological replicates.

JC1 imaging:

hRGCs were seeded in MG coated MatTek dishes at 40,000 cells per dish and maintained for 3 days. On the day of experiment, cells were incubated with 250 μl of JC1 media (1:100 in iNS) for 30 minutes in the incubator, then an additional 1.75ml of dilute JC1 (1:1000 in iNS) was added to the dish. The dish was then transferred to the live cell chamber (5% CO_2, 37°C, Tokai Hit) and confocal images were acquired prior to (before) and 10 minutes after CCCP (10 μM) treatment using Zeiss LSM700 with 63x/1.4 oil objective. Analysis was carried out using ImageJ with sum projections of red and green channels normalized to cell

area. The red fluorescence from the tdTomato expressed by the hRGCs was much less intense than the JC1 red staining of mitochondria, thus the red fluorescence measured from the cytoplasm was considered background and subtracted out of the images for measurements.

Seahorse analysis:

The 96 well seahorse plate was coated with MG and hRGCs were seeded at 250,000 cells per well and maintained for 2 days. 24 hours before measurements, media was exchanged with 100 µl iNS with 1 µg/ml BX795 or equivalent vehicle control DMSO. A day prior to the assay, the sensor cartridge was fully submerged with 200 µl of sterile water to hydrate it overnight in a non-CO_2, 37°C incubator. The next day, sterile water was replaced with pre-warmed XF calibrant buffer and the sensors were again submerged and incubated in the non-CO_2, 37°C incubator for 45-60 minutes. Seahorse media was made by adding stock solutions to seahorse media (XF DMEM) to have final concentrations of 21.25 mM glucose, 0.36 mM sodium pyruvate, and 1.25 mM L-glutamine (Agilent), with pH adjusted to 7.38-7.42. 20 µM Oligomycin, 20 µM FCCP, and 2.5 µg/ml Rotenone plus 5 µM Antimycin A solutions were then prepared in Seahorse media. In the hRGC seahorse plate, iNS media was carefully exchanged to seahorse media by removing, 60 µl iNS from all wells and adding 140 µl of Seahorse media. Next, 140 µl of the mixed media was removed by pipette and then an additional 140 µl seahorse media was added to each well to have a final volume of 180 µl. 180 µl of Seahorse media was then added to any empty wells. The plate was placed in Incucyte S3 (Sartorius) and one image of each well was taken for cell area normalization using brightfield and red fluorescence (tdTomato) channels. The RGC seahorse plate was then placed into non-CO_2, 37°C incubator for at least 45 min. For Mito Stress Test assay, the reagents were added into their respective ports in the cartridge with the final concentrations in the wells of 2.0 µM for Oligomycin, 2.0 µM for FCCP (optimal concentration from FCCP titration), and 0.25 µg/ml Rotenone plus 0.5 µM Antimycin A. After loading all ports, the cartridge was placed into the XFe96 analyzer (Agilent) and run for calibration. After the machine calibrations were successful, the RGC seahorse plate was placed into the machine and the Mito

Stress Test Assay was run. Cell area from incucyte images were measured using image J and extrapolated for the total cell area in each well for normalization. The assay results were then exported into Excel using Seahorse Wave Desktop software (Agilent) for analysis.

Cell viability and caspase activity:

hRGCs were seeded at 25,000 cells per well of a 96 well clear bottom black walled plate and maintained for 3 days. The cells were then treated with 1µg/ml BX795 or equivalent volume of DMSO vehicle control for 24h. The cell viability and caspase activity were measured using the ApoTox-Glo Triplex assay kit (Promega). Assay buffer, GF-AFC substrate and bis-AAF-R110 substrate were thawed at 37°C and 10µl of GF-AFC substrate and bis-AAF-R110 substrate were added into 2.0 ml of assay buffer and vortexed until dissolved to make the viability-cytotoxicity reagent. 20µl of viability-cytotoxicity reagent was added to all wells, and briefly mixed. The plate was incubated at 37°C for 30 minutes before measuring the fluorescence at 400nm/505nm (Ex/Em) for viability. Next, 100µl of Caspase-Glo® 3/7 reagent was added to all wells and incubated for 30 minutes at room temperature before measuring luminescence (Caspase). Measurements were normalized to DMSO control.

Electron Microscopy:

hRGCs were seeded at 250,000 cells per well on MG coated 6-well plates and maintained for 3 days. The cells were then treated with 1µg/ml BX795 or equivalent DMSO for 24 hours. Media was aspirated, 500µl of fixative solution (3% Glutaraldehyde, 0.1M Cacodylate) was added, and the cells were incubated for 15 minutes. hRGCs were then scraped and pelleted by centrifugation at 10,000 RPM for 20 minutes. The pellets were fixed overnight at 4°C, then rinsed the next day in 0.1M cacodylate buffer, followed by post fixation with 1% osmium tetroxide, 0.1M cacodylate buffer for 1 hour. After rinsing again with 0.1M cacodylate buffer, the cell pellets were dehydrated through a series of graded ethyl alcohols from 70 to 100%, and 2 changes of 100% acetone. The cell pellets were then infiltrated with a 50:50 mixture of acetone and embedding resin (Embed 812, Electron Microscopy Sciences, Hatfield, PA) for 72h. Specimen vial lids

were then removed, and acetone allowed to evaporate off for 3 hours. Then the pellets were embedded in a fresh change of 100% embedding resin. Following polymerization overnight at 60°C the blocks were then ready for sectioning. All procedures were done in centrifuge tubes including the final embedding. Sections with cut at 85nm, placed on copper grids, stained with saturated uranyl acetate, viewed, and imaged on a Tecnai Spirit (ThermoFisher, Hillsboro, OR) equipped with an AMT CCD camera (Advanced Microscopy Techniques, Danvers, MA). 49000X images were analyzed using Image J to measure mitochondrial characteristics and then normalized to cytoplasmic area (mitochondrial number and area) or ratio of major to minor axis for aspect ratio.

Quantification and Statistical analysis:

Statistical tests between two samples were done by Student's *t-test*. For three or more conditions, ANOVA with either Tukey's post-hoc tests to adjust for multiple testing among all groups or Dunnett's tests for comparisons of multiple groups against a control were done using GraphPad Prism 9.0 software.

Data availability

All cell lines and data used during the current study are available from the corresponding author upon reasonable request.

Code availability

Data analyzed using commercially available software, no code has been developed for the current study.

References

1. Kann, O. & Kovács, R. Mitochondria and neuronal activity. *American Journal of Physiology - Cell Physiology* vol. 292 (2007).
2. Yu-Wai-Man, P., Griffiths, P. G. & Chinnery, P. F. Mitochondrial optic neuropathies - Disease mechanisms and therapeutic strategies. *Progress in Retinal and Eye Research* vol. 30 81–114 (2011).
3. Reeve, A. K. *et al.* Mitochondrial dysfunction within the synapses of substantia nigra neurons in Parkinson's disease. *npj Parkinson's Disease* **4**, (2018).
4. Kong, J. & Xu, Z. Massive mitochondrial degeneration in motor neurons triggers the onset of amyotrophic lateral sclerosis in mice expressing a mutant SOD1. *Journal of Neuroscience* **18**, (1998).
5. Man, P. Y. W., Turnbull, D. M. & Chinnery, P. F. Leber hereditary optic neuropathy. *Journal of Medical Genetics* vol. 39 (2002).
6. Zanna, C. *et al.* OPA1 mutations associated with dominant optic atrophy impair oxidative phosphorylation and mitochondrial fusion. *Brain* **131**, (2008).
7. Wolf, C. *et al.* Evaluation of nine candidate genes in patients with normal tension glaucoma: A case control study. *BMC Medical Genetics* **10**, 91 (2009).
8. Rezaie, T. *et al.* Adult-onset primary open-angle glaucoma caused by mutations in optineurin. *Science (1979)* **295**, 1077–1079 (2002).
9. Ayala-Lugo, R. M. *et al.* Variation in optineurin (OPTN) allele frequencies between and within populations. *Mol Vis* **13**, 151–63 (2007).
10. Salminen, A. & Kaarniranta, K. AMP-activated protein kinase (AMPK) controls the aging process via an integrated signaling network. *Ageing Research Reviews* vol. 11 (2012).
11. Zhao, P. *et al.* TBK1 at the Crossroads of Inflammation and Energy Homeostasis in Adipose Tissue. *Cell* **172**, 731-743.e12 (2018).
12. Mattson, M. P. & Arumugam, T. v. Hallmarks of Brain Aging: Adaptive and Pathological Modification by Metabolic States. *Cell Metabolism* vol. 27 (2018).
13. Jäer, S., Handschin, C., St-Pierre, J. & Spiegelman, B. M. AMP-activated protein kinase (AMPK) action in skeletal muscle via direct phosphorylation of PGC-1α. *Proc Natl Acad Sci U S A* **104**, (2007).
14. Zhao, P. & Saltiel, A. R. Interaction of Adipocyte Metabolic and Immune Functions Through TBK1. *Frontiers in Immunology* vol. 11 (2020).
15. Peng, Y. R. *et al.* Molecular Classification and Comparative Taxonomics of Foveal and Peripheral Cells in Primate Retina. *Cell* **176**, 1222-1237.e22 (2019).
16. Sluch, V. M. *et al.* Enhanced Stem Cell Differentiation and Immunopurification of Genome Engineered Human Retinal Ganglion Cells. *Stem Cells Translational Medicine* **6**, 1972–1986 (2017).
17. Sluch, V. M. *et al.* Differentiation of human ESCs to retinal ganglion cells using a CRISPR engineered reporter cell line. *Scientific Reports* **5**, (2015).
18. Zhang, K. Y. *et al.* Role of the Internal Limiting Membrane in Structural Engraftment and Topographic Spacing of Transplanted Human Stem Cell-Derived Retinal Ganglion Cells. *Stem Cell Reports* **16**, 149–167 (2021).
19. Das, A., Bell, C. M., Berlinicke, C. A., Marsh-Armstrong, N. & Zack, D. J. Programmed switch in the mitochondrial degradation pathways during human retinal ganglion cell differentiation from stem cells is critical for RGC survival. *Redox Biology* (2020) doi:10.1016/j.redox.2020.101465.
20. Ohlemacher, S. K. *et al.* Stepwise Differentiation of Retinal Ganglion Cells from Human Pluripotent Stem Cells Enables Analysis of Glaucomatous Neurodegeneration. *Stem Cells* **34**, 1553–1562 (2016).

21. VanderWall, K. B. *et al.* Retinal Ganglion Cells With a Glaucoma OPTN(E50K) Mutation Exhibit Neurodegenerative Phenotypes when Derived from Three-Dimensional Retinal Organoids. *Stem Cell Reports* **15**, 52–66 (2020).
22. Yu, D. Y. *et al.* Retinal ganglion cells: Energetics, compartmentation, axonal transport, cytoskeletons and vulnerability. *Progress in Retinal and Eye Research* vol. 36 (2013).
23. Sivandzade, F., Bhalerao, A. & Cucullo, L. Analysis of the Mitochondrial Membrane Potential Using the Cationic JC-1 Dye as a Sensitive Fluorescent Probe. *Bio-Protocol* **9**, (2019).
24. Holloszy, J. O. Regulation of mitochondrial biogenesis and GLUT4 expression by exercise. *Comprehensive Physiology* vol. 1 921–940 (2011).
25. Mattson, M. P., Moehl, K., Ghena, N., Schmaedick, M. & Cheng, A. Intermittent metabolic switching, neuroplasticity and brain health. *Nature Reviews Neuroscience* vol. 19 81–94 (2018).
26. Wu, Z. *et al.* Mechanisms controlling mitochondrial biogenesis and respiration through the thermogenic coactivator PGC-1. *Cell* **98**, 115–124 (1999).
27. Gureev, A. P., Shaforostova, E. A. & Popov, V. N. Regulation of mitochondrial biogenesis as a way for active longevity: Interaction between the Nrf2 and PGC-1α signaling pathways. *Frontiers in Genetics* vol. 10 (2019).
28. Scarpulla, R. C., Vega, R. B. & Kelly, D. P. Transcriptional integration of mitochondrial biogenesis. *Trends in Endocrinology and Metabolism* vol. 23 459–466 (2012).
29. Hardie, D. G. AMP-activated protein kinase-an energy sensor that regulates all aspects of cell function. *Genes and Development* vol. 25 1895–1908 (2011).
30. Shaw, R. J. *et al.* The tumor suppressor LKB1 kinase directly activates AMP-activated kinase and regulates apoptosis in response to energy stress. *Proc Natl Acad Sci U S A* **101**, 3329–3335 (2004).
31. Li, F. *et al.* Structural insights into the interaction and disease mechanism of neurodegenerative disease-associated optineurin and TBK1 proteins. *Nature Communications* **7**, (2016).
32. Minegishi, Y. *et al.* Enhancedoptineurin E50k-TBK1 interaction evokes protein insolubility and initiates familial primary open-angle glaucoma. *Human Molecular Genetics* **22**, 3559–3567 (2013).
33. Clark, K., Plater, L., Peggie, M. & Cohen, P. Use of the pharmacological inhibitor BX795 to study the regulation and physiological roles of TBK1 and IκB Kinase ∈:A distinct upstream kinase mediates ser-172 phosphorylation and activation. *Journal of Biological Chemistry* **284**, (2009).
34. Minegishi, Y., Nakayama, M., Iejima, D., Kawase, K. & Iwata, T. Significance of optineurin mutations in glaucoma and other diseases. *Progress in Retinal and Eye Research* vol. 55 149–181 (2016).
35. Ritch, R. *et al.* TBK1 gene duplication and normal-tension glaucoma. *JAMA Ophthalmology* **132**, 544–548 (2014).
36. Fingert, J. H. *et al.* Transgenic TBK1 mice have features of normal tension glaucoma. *Hum Mol Genet* **26**, 124–132 (2017).
37. Javadov, S., Chapa-Dubocq, X. & Makarov, V. Different approaches to modeling analysis of mitochondrial swelling. *Mitochondrion* vol. 38 (2018).
38. Quigley, H. A. Understanding Glaucomatous Optic Neuropathy: The Synergy Between Clinical Observation and Investigation. *Annual review of vision science* vol. 2 235–254 (2016).
39. Desler, C. *et al.* Is there a link between mitochondrial reserve respiratory capacity and aging? *Journal of Aging Research* vol. 2012 (2012).
40. Hardie, D. G., Ross, F. A. & Hawley, S. A. AMPK: A nutrient and energy sensor that maintains energy homeostasis. *Nature Reviews Molecular Cell Biology* vol. 13 (2012).
41. Daval, M., Foufelle, F. & Ferré, P. Functions of AMP-activated protein kinase in adipose tissue. *Journal of Physiology* vol. 574 (2006).
42. Eells, J. T. Mitochondrial dysfunction in the aging retina. *Biology* vol. 8 (2019).
43. Taft, J. *et al.* Human TBK1 deficiency leads to autoinflammation driven by TNF-induced cell death. *Cell* **184**, (2021).

44. Reilly, S. M. *et al.* An inhibitor of the protein kinases TBK1 and IKK-ε improves obesity-related metabolic dysfunctions in mice. *Nature Medicine* **19**, (2013).
45. Richter, B. *et al.* Phosphorylation of OPTN by TBK1 enhances its binding to Ub chains and promotes selective autophagy of damaged mitochondria. *Proc Natl Acad Sci U S A* **113**, 4039–4044 (2016).
46. Cai, Q. & Jeong, Y. Y. Mitophagy in Alzheimer's Disease and Other Age-Related Neurodegenerative Diseases. *Cells* **9**, 150 (2020).
47. Harding, O. *et al.* ALS- And FTD-associated missense mutations in TBK1 differentially disrupt mitophagy. *Proc Natl Acad Sci U S A* **118**, (2021).

Figure Legends

Figure 1. hRGCs produce more mitochondria to maintain homeostasis under mitochondrial damage. (**a)** Representative WB images of hRGCs treated with 10 μM CCCP for indicated time. (**b, c**) Quantification of average western blot band intensities of Tom70 protein normalized to GAPDH, n=3-6. (**d)** Representative 63x confocal immunofluorescence images of H7-hRGCs with Tom20, tdTomato, and DAPI after indicated CCCP timepoints. Scale bars are 5 μm. (**e**) Quantification of Tom20 intensity per cell area from sum projections of confocal z-stacks. (**f**) Mitochondria were labelled in hRGCs with the live cell MTDR dye followed by a wash, CCCP treatment without MTDR and quantification of average mitochondrial mass in single cell by flow cytometer at the indicated time points. n=3. (**g**) Mitochondria in hRGCs were labelled with MTDR, then treated with CCCP for 3h, washed, and incubated with fresh media with MTDR to label newly synthesized mitochondria, quantified by flow cytometer. *, p-value < 0.05, **, p-value < 0.01, ***, p-value < 0.001, ****, p-value < 0.0001 One-way Anova with Dunnett's using comparison to DMSO of respective cell line (**e, f**). One-way Anova with Tukey's (**g**). n=3. Error bars are SEM.

Figure 2. hRGCs degrade damaged and produce healthy mitochondria under stress. (**a**) Representative confocal sum projections of respective green and red channels before and 10 min after CCCP treatment. JC1 dye was present 30min before CCCP and during treatments. Scale bars are 5 μm. **(b)** Quantification of sum projections of the total intensity normalized to cell area of JC1 green, (**c**) JC1 red, and (**d**) the ratio of red-to-green. Error bars are SEM. Two-way Anova with Tukey's, ****, p-value < 0.0001, **, p-value < 0.01, *, p-value < 0.05, n = 17-42 hRGCs.

Figure 3. Mitochondrial damage activates AMPK-PGC-1α biogenesis axis in hRGCs. (**a-d**) Mitochondrial biogenesis gene expressions in the indicated hRGCs after 24h CCCP (10 μM) treatment. ΔΔCt fold changes were measured with-respect-to (w.r.t) GAPDH and DMSO. Error bars are

SEM. n=3, 3 technical repeats averaged for each biological repeat. (**e**) Representative western blot images of H7-hRGCs treated with 10 μM CCCP for the indicated timepoints. (**f-i**) Quantification of average western blot band intensities of the indicated proteins normalized to corresponding actin and then with DMSO control, n=3. Student's *t-test*, *, p-value < 0.05 **, p-value < 0.01.

Figure 4. TBK1 inhibition mediated AMPK activation is defective in E50K hRGCs. (a) Confocal immunofluorescence images of mitochondria (Tom20) and OPTN. Scale bars are 5 μm. **(b)** Quantification of OPTN aggregate size, (**c, d)** Tom20 intensity from the sum projection of confocal z-stacks normalized to cell area and then to DMSO control, n=10 images per condition. Error bars are SEM. (**e, g**) Representative western blot images of indicated proteins from corresponding hRGCs treated with 1 μg/ml BX795 of Tom70. (**f, h, i**) Average band intensity first normalized to corresponding GAPDH and then to DMSO control, n=3. **, p-value < 0.01, *, p-value < 0.05. Student's *t-test* (c, d). One-way Anova with Dunnett's using comparison to DMSO of respective cell line (**b, i**).

Figure 5. TBK1 inhibition improves mitochondrial coverage and morphology in hRGCs. (**a**) Confocal immunofluorescence images of mitochondria in hRGCs. Scale bars are 10 μm. (**b**) Quantification of Tom20 intensity normalized to cell area, n = 10-25. (**c**) TEM images of H7-hRGC^{WT} and H7-hRGC^{E50K} after 24h treatments of DMSO or BX79524h, at 49000X magnification. Asterisks represent mitochondria. Scale bar = 200nm. (**d-g**) Quantification of total mitochondrial area w.r.t. cytoplasmic area (**d**), perimeter length (**e**), major axis length (**f**) and minor axis length (**g**). Student's t-test between independent variables, **** p-value <0.0001, ** p-value <0.01, * p-value <0.05, n=15-24.

Figure 6. TBK1 inhibition enhances respiratory capacity and cell survival for hRGCs. (a-b) Measurement of cell area normalized OCR from Seahorse Mito Stress Test after addition of 2 μM Oligomycin (Oligo), 2 μM FCCP, and 0.25 μg/ml Rotenone plus 0.5 μM AntimycinA (Rot/AA) at indicated timepoints to the indicated cells. (**c**) Spare respiratory capacity measurements after 24h

treatment with 1μg/ml BX795. Error bars are SEM, n=6. (**d**) Cell viability **(e)** and Caspase-3/7 activity were measured using ApoToxGlo-Triplex assay kit in hRGCs after 24h DMSO or 1 μg/ml BX treatments. Error bars are SEM. Student's *t-test*, *, p-value < 0.05, **, p-value < 0.01, n = 15-22.

Supplementary Figure 1. hRGC differentiation and CRISPR mutated OPTN^{E50K} stem cell lines. (a) Shown are confocal immunofluorescence images of hRGCs against neuronal marker TUBB3 and (**b**) RGC specific marker RBPMS. Scale bars are 10 μm. (**c**) Sanger sequencing chromatograms show the E50 sequence and the homozygous E50K mutation in the H7-ESCs.

Supplementary Figure 2. Flow cytometry measurement of MTDR labelled mitochondrial mass in hRGCs. (a, d) Live hRGCs were gated from the total population measured after DMSO and 15 min 10 μM CCCP treatments. (**b, e**) From the live cells, singlet populations were gated. **(c, f)** From singlet populations, average MTDR intensity were measured for tdTomato (red) and MTDR (far red) positive hRGCs. CCCP treatment reduces MTDR positive mitochondrial mass as shown by the left shift of MTDR positive cells **(f)**.

Figure 1

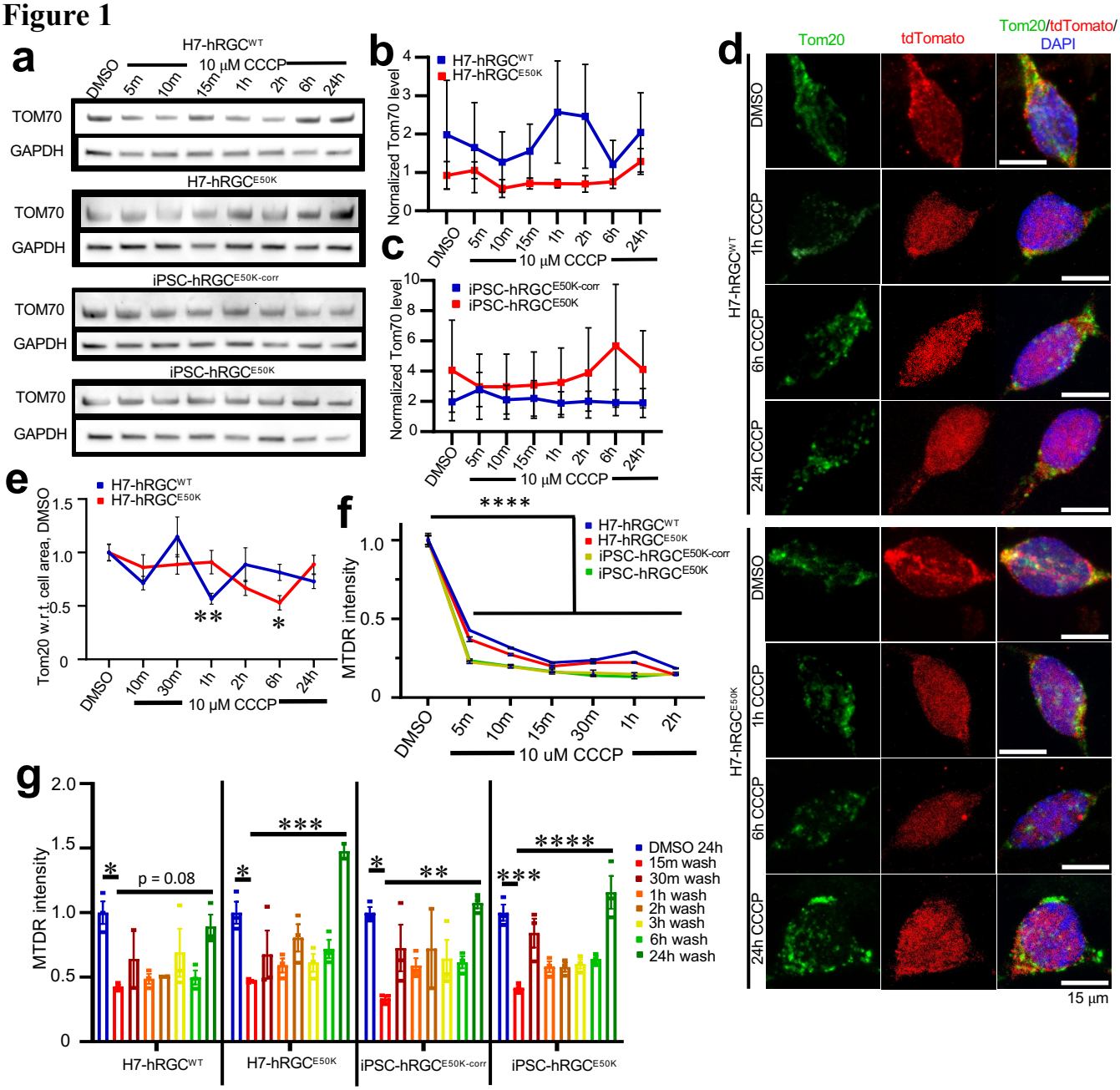
a
H7-hRGC^WT
10 μM CCCP
DMSO
5m
10m
15m
1h
2h
6h
24h
TOM70
GAPDH
H7-hRGC^E50K
iPSC-hRGC^E50K-corr
iPSC-hRGC^E50K
b
Normalized Tom70 level
c
d
Tom20
tdTomato
Tom20/tdTomato/DAPI
1h CCCP
6h CCCP
24h CCCP
15 μm
e
Tom20 w.r.t. cell area, DMSO
f
MTDR intensity
10 uM CCCP
g
p = 0.08
DMSO 24h
15m wash
30m wash
1h wash
2h wash
3h wash
6h wash
24h wash

Figure 2

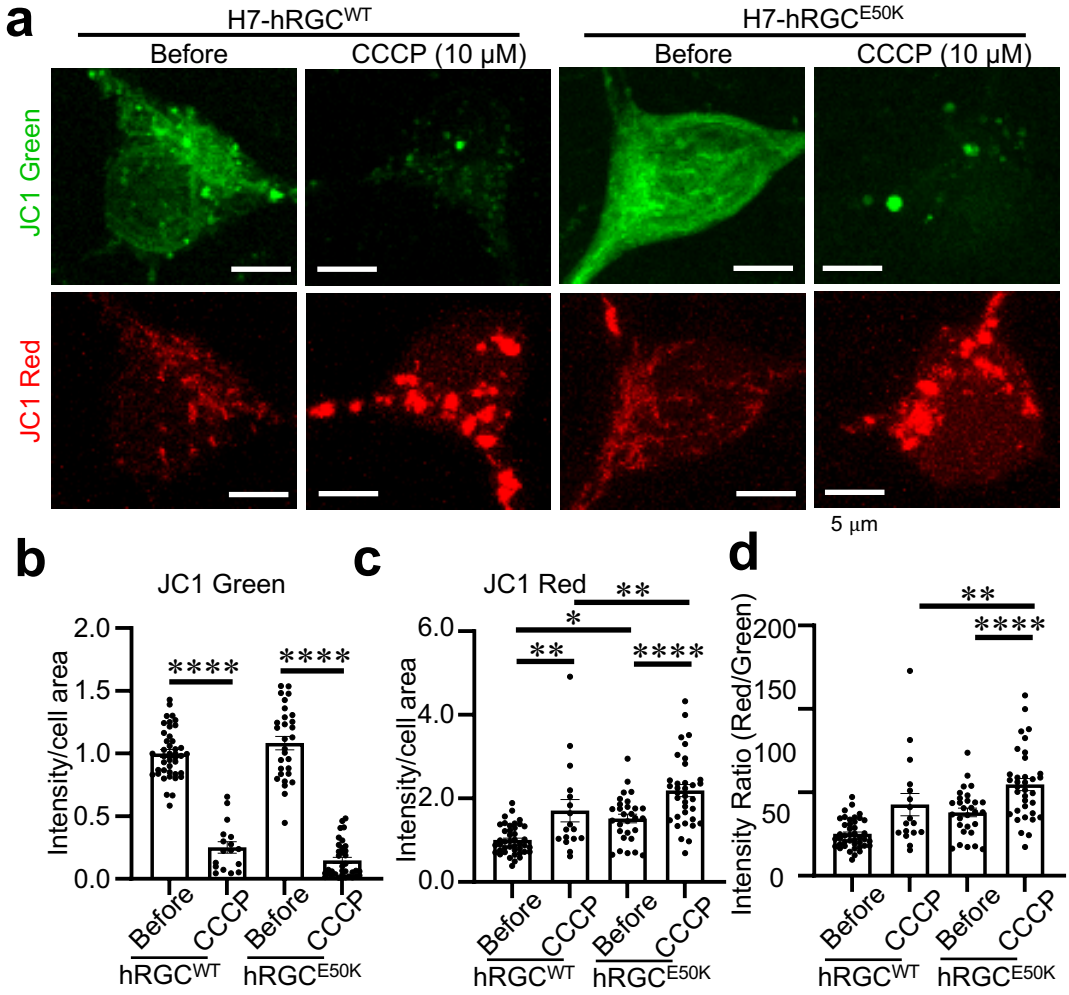
a
H7-hRGC^WT
H7-hRGC^E50K
Before
CCCP (10 μM)
Before
CCCP (10 μM)
JC1 Green
JC1 Red
5 μm
b
JC1 Green
Intensity/cell area
2.0
1.5
1.0
0.5
0.0
****
****
Before
CCCP
Before
CCCP
hRGC^WT
hRGC^E50K
c
JC1 Red
Intensity/cell area
6.0
4.0
2.0
0.0
**
*
**
****
Before
CCCP
Before
CCCP
hRGC^WT
hRGC^E50K
d
Intensity Ratio (Red/Green)
200
150
100
50
0
**
****
Before
CCCP
Before
CCCP
hRGC^WT
hRGC^E50K

Figure 3

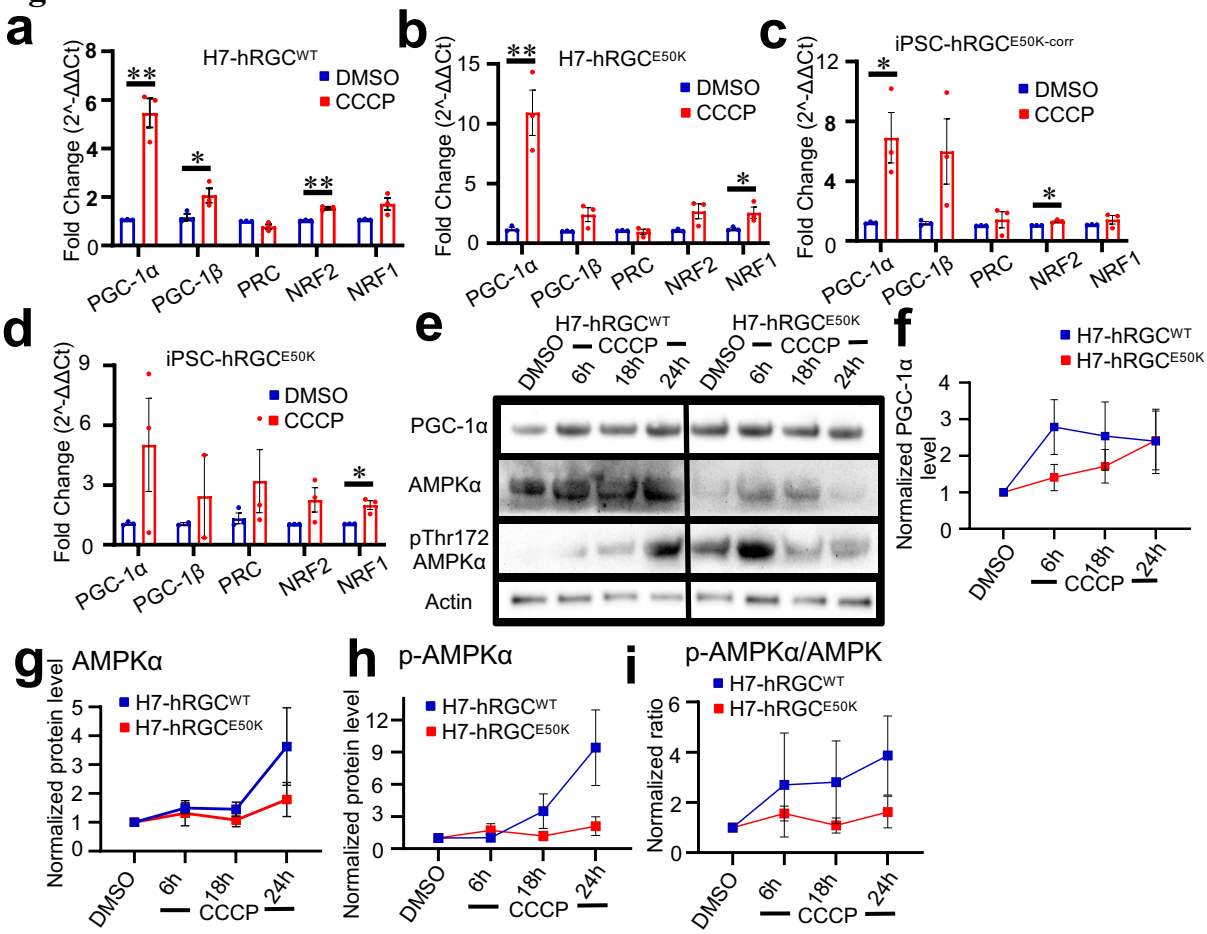
a
H7-hRGCWT
DMSO
CCCP
Fold Change (2^-ΔΔCt)
PGC-1α
PGC-1β
PRC
NRF2
NRF1
b
H7-hRGCE50K
c
iPSC-hRGCE50K-corr
d
iPSC-hRGCE50K
e
H7-hRGCWT
H7-hRGCE50K
DMSO
6h
18h
24h
CCCP
PGC-1α
AMPKα
pThr172 AMPKα
Actin
f
Normalized PGC-1α level
g
AMPKα
Normalized protein level
h
p-AMPKα
i
p-AMPKα/AMPK
Normalized ratio

Figure 4

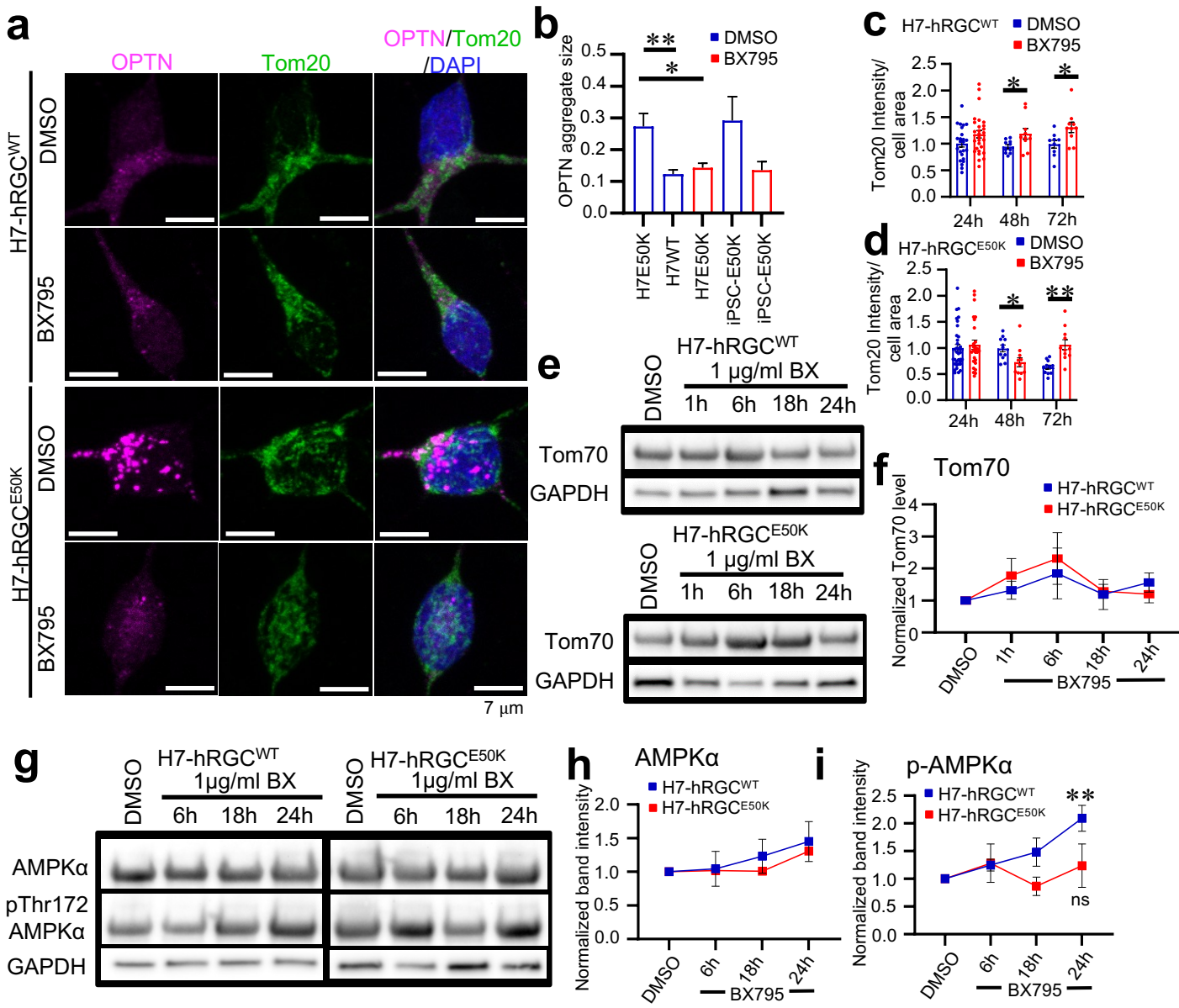
a
OPTN
Tom20
OPTN/Tom20 /DAPI
H7-hRGC^WT
DMSO
BX795
H7-hRGC^E50K
DMSO
BX795
7 μm
b
OPTN aggregate size
DMSO
BX795
H7E50K
H7WT
H7E50K
iPSC-E50K
iPSC-E50K
c
H7-hRGC^WT
DMSO
BX795
Tom20 Intensity/ cell area
24h
48h
72h
d
H7-hRGC^E50K
DMSO
BX795
Tom20 Intensity/ cell area
24h
48h
72h
e
H7-hRGC^WT
1 μg/ml BX
DMSO
1h
6h
18h
24h
Tom70
GAPDH
H7-hRGC^E50K
1 μg/ml BX
DMSO
1h
6h
18h
24h
Tom70
GAPDH
f
Tom70
H7-hRGC^WT
H7-hRGC^E50K
Normalized Tom70 level
DMSO
1h
6h
18h
24h
BX795

g
DMSO
H7-hRGC^WT
1μg/ml BX
6h
18h
24h
DMSO
H7-hRGC^E50K
1μg/ml BX
6h
18h
24h
AMPKα
pThr172 AMPKα
GAPDH
h
AMPKα
H7-hRGC^WT
H7-hRGC^E50K
Normalized band intensity
DMSO
6h
18h
24h
BX795
i
p-AMPKα
H7-hRGC^WT
H7-hRGC^E50K
Normalized band intensity
ns
DMSO
6h
18h
24h
BX795

Figure 5

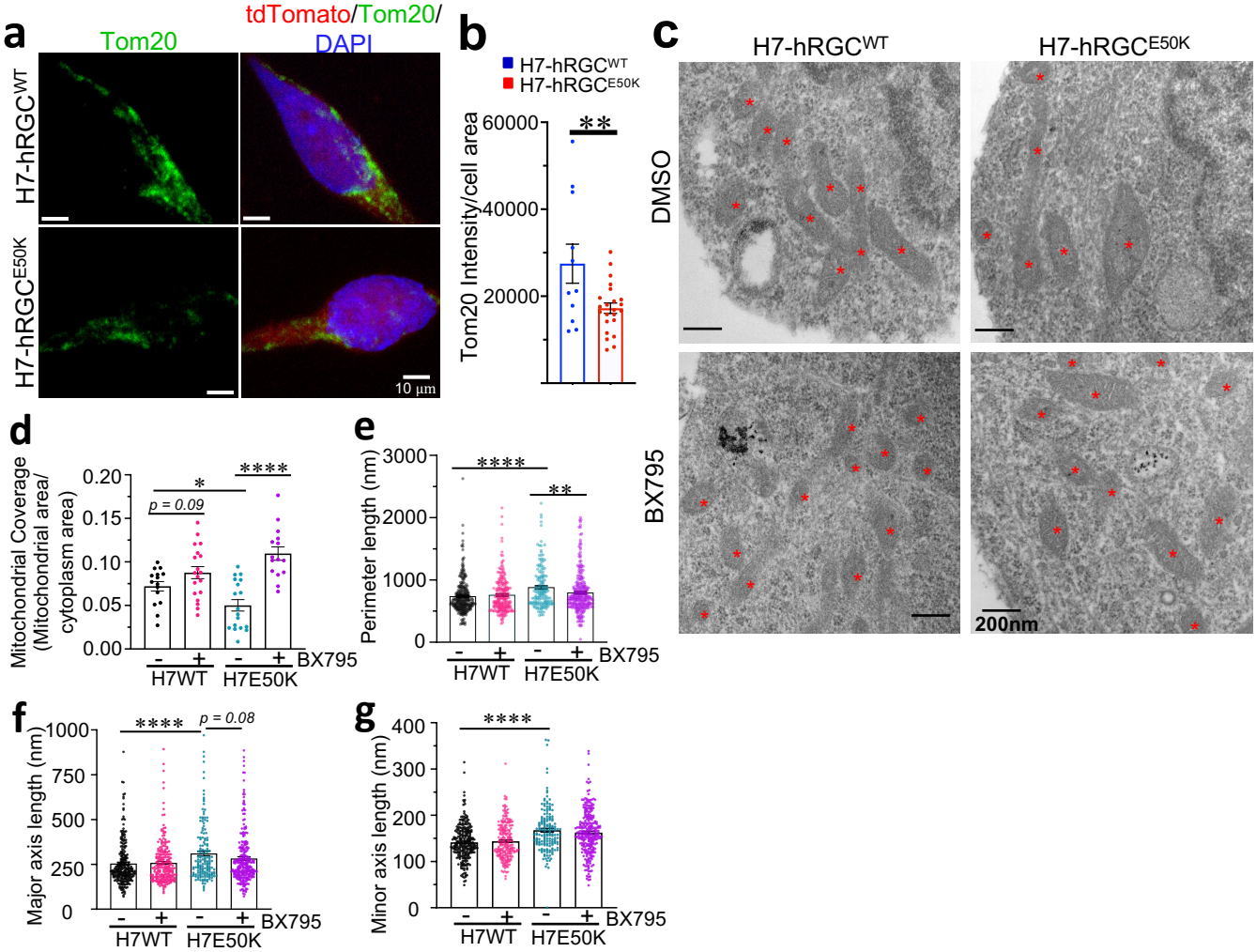
a
Tom20
tdTomato/Tom20/
DAPI
H7-hRGC^WT
H7-hRGC^E50K
10 µm
b
H7-hRGC^WT
H7-hRGC^E50K
Tom20 Intensity/cell area
60000
40000
20000
**
c
H7-hRGC^WT
H7-hRGC^E50K
DMSO
BX795
200nm
d
Mitochondrial Coverage
(Mitochondrial area/
cytoplasm area)
0.20
0.15
0.10
0.05
0.00
*
****
p = 0.09
-
+
-
+
BX795
H7WT
H7E50K
e
Perimeter length (nm)
3000
2000
1000
0
****
**
-
+
-
+
BX795
H7WT
H7E50K
f
Major axis length (nm)
1000
750
500
250
0
****
p = 0.08
-
+
-
+
BX795
H7WT
H7E50K
g
Minor axis length (nm)
400
300
200
100
0
****
-
+
-
+
BX795
H7WT
H7E50K

Figure 6

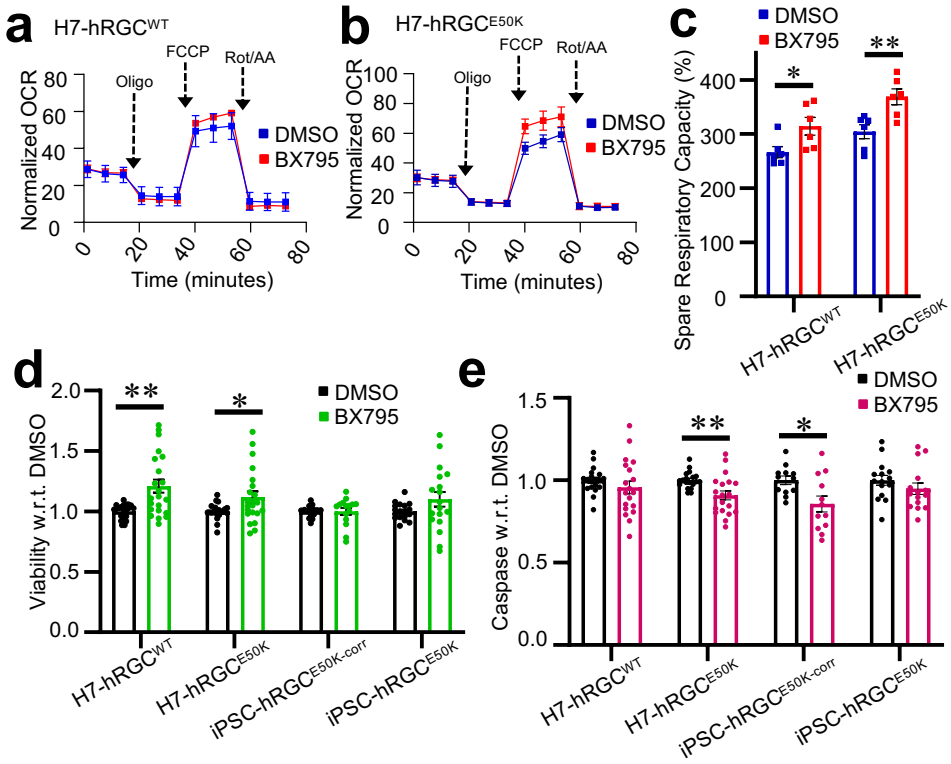
a
H7-hRGC^WT
Oligo
FCCP
Rot/AA
Normalized OCR
Time (minutes)
DMSO
BX795
b
H7-hRGC^E50K
Oligo
FCCP
Rot/AA
Normalized OCR
Time (minutes)
DMSO
BX795
c
DMSO
BX795
Spare Respiratory Capacity (%)
H7-hRGC^WT
H7-hRGC^E50K
d
DMSO
BX795
Viability w.r.t. DMSO
H7-hRGC^WT
H7-hRGC^E50K
iPSC-hRGC^E50K-corr
iPSC-hRGC^E50K
e
DMSO
BX795
Caspase w.r.t. DMSO
H7-hRGC^WT
H7-hRGC^E50K
iPSC-hRGC^E50K-corr
iPSC-hRGC^E50K

Supplementary Figure 1

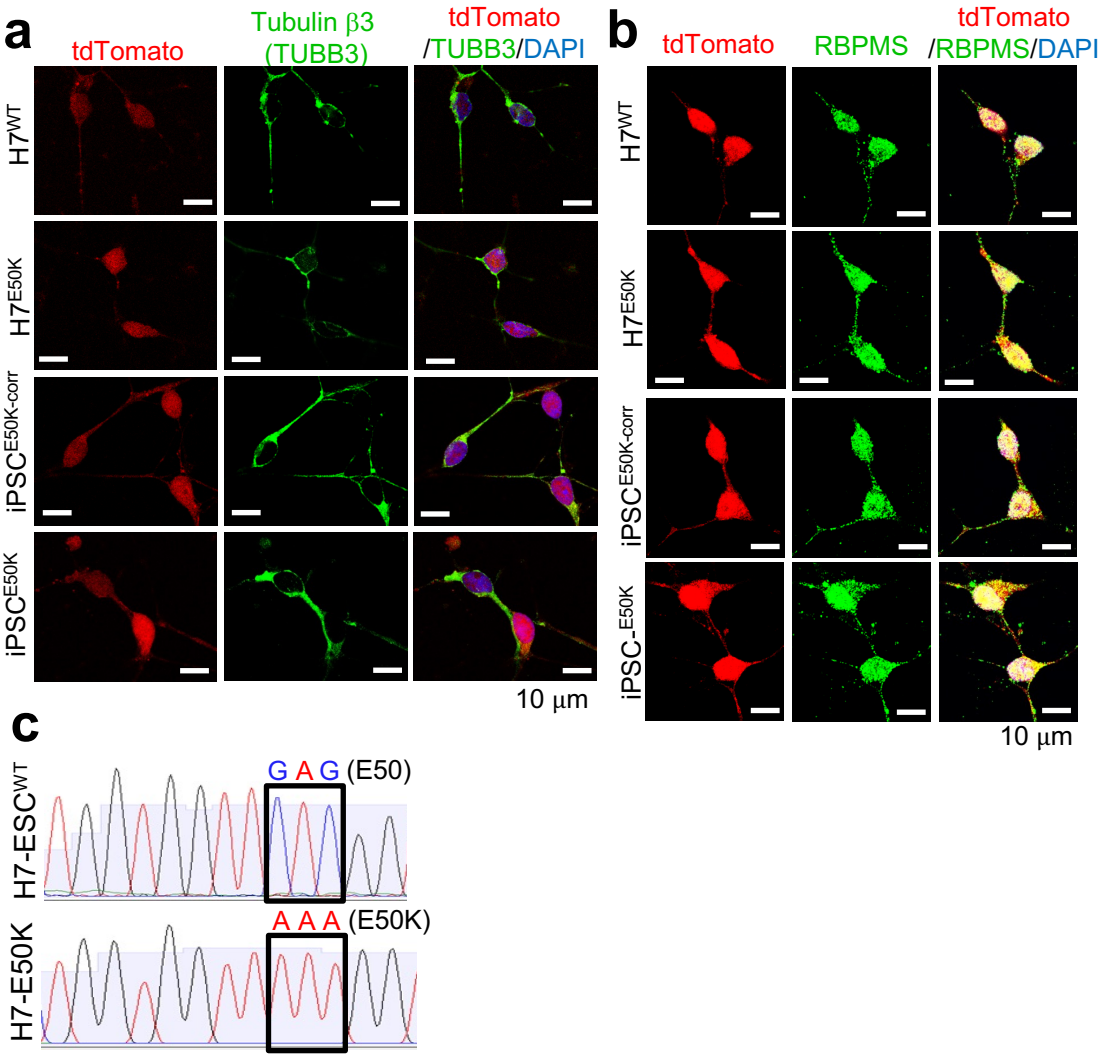

Supplementary Figure 2

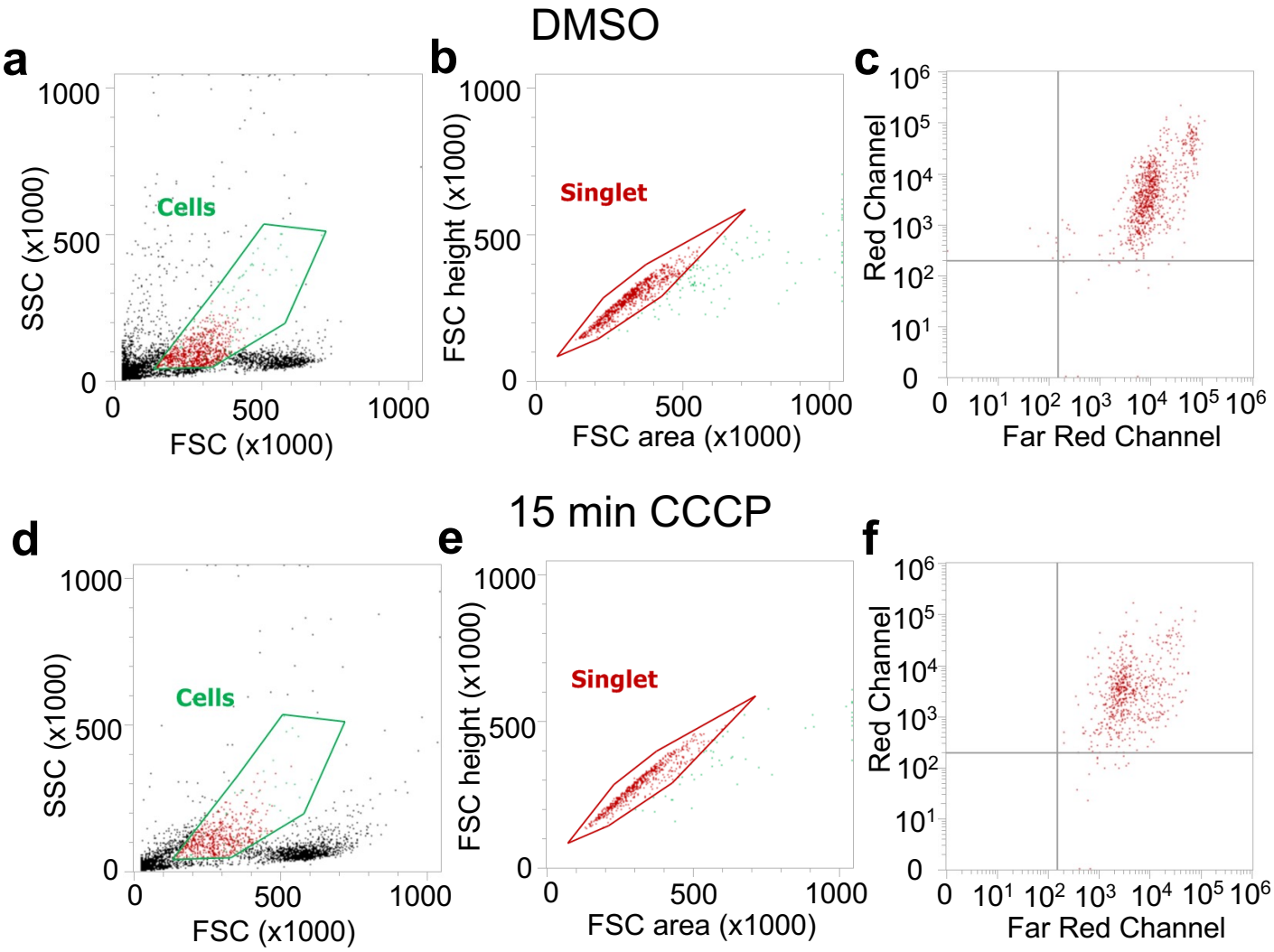

Supplemental table S1: list of reagents, software, antibodies, and primers (qPCR)

REAGENTS AND ASSAY KITS		
Reagent	**Manufacturer**	**Catalog Number**
Matrigel	Corning	CB40230
Gentle Cell Dissociation Reagent	Stem Cell Technology	7174
mTeSR1	Stem Cell Technology	85850
Accutase	Sigma	A6964
Blebbistatin	Sigma	B0560
DMEM/F-12	Thermo Scientific	11330032
Neurobasal media	Thermo Scientific	21103049
GlutaMAX supplement (100X)	Invitrogen	35050061
Antibiotic-Antimycotic	Thermo Scientific	15240062
B27 supplement	Thermo Scientific	17504044
N2 supplement	Thermo Scientific	17502048
Nicotinamide	Sigma	N3376
IDE2	Tocris	4016
Forskolin	Stem cell technologies	3828S
Dorsomorphin	Stem cell technologies	P5499
DAPT	Sigma	D5942
MACS kit	Miltenyi Biotec	130-091-051 130-042-108
Dimethylsulphoxide (DMSO)	Sigma	276855
Carbonyl cyanide-3-chlorophenylhydrazone (CCCP)	Sigma	C2759
BX-795 hydrochloride	Sigma	SML0694
M-PER mammalian protein extraction reagent	Thermo Scientific	78503
Halt protease and phosphatase inhibitor cocktail (100X)	Thermo Scientific	1861281
0.5 M EDTA solution (100X)	Thermo Scientific	1861274
DC Protein Assay Kit II	Bio-Rad	5000112
Laemmli buffer (4X)	Bio-Rad	1610747
BioRad Mini-PROTEAN TGX precast gels	Bio-Rad	4561024 4561025
Running buffer (10x Tris/Glycine/SDS)	Bio-Rad	1610732
Transfer buffer (10x Tris/Glycine)	Bio-Rad	1610734
Immuno-blot PVDF membrane	Bio-Rad	1620260
Methanol	Sigma	34860
TBS buffer 20x	VWR	J640
Tween 20	Sigma	P9416
Clarity Max Western ECL substrate	Bio-Rad	1705060
DAPI	Molecular Probes	D1206
Paraformaldehyde 16% solution, EM grade	Electron Microscopy Sciences	15710
Triton-X-100	Sigma	T8787
Donkey Serum	Sigma	D9663
RNeasy Mini Kit	Qiagen	74104
5x all-in-one RT MasterMix (with AccuRTGenomic DNA Removal kit)	Applied biological materials	G492
BlasTaq 2X qPCR MasterMix	Abcam	G891
JC1 dye	Cayman Chemicals	10009172

ApoTox-Glo™ Triplex Assay	Promega	G6320
Seahorse XF Cell Mito Stress Test Kit	Agilent	103015-100
Antibody	**Manufacturer**	**Catalog Number**
β-actin (rabbit)	Cell signaling technologies	4967S
GAPDH (rabbit monoclonal)	Cell signaling technologies	2118S
TOM70 (rabbit)	Novas Biologicals	NBP1-87863
PGC 1α (rabbit)	Abcam	Ab191838
PGC 1β (rabbit)	Abcam	Ab176328
AMPKα (rabbit)	Cell signaling technologies	2532S
Phospho-AMPKα (Thr172) (rabbit monoclonal)	Cell signaling technologies	2535T
Goat anti-rabbit-IgG1-HRP-linked Ab	Cell signaling technologies	7074S
Optineurin (C-Term) (rabbit polyclonal)	Cayman Chemicals	100000
TOM 20 (mouse)	Santa Cruz	sc-17764
Donkey anti-mouse Alexa Fluor 488	Invitrogen	A12379
Donkey anti-rabbit Alexa Fluor 647	Invitrogen	A31573
SOFTWARE AND ALGORITHMS		
ImageJ	NIH	
Prism version 9	GraphPad	
Zen Microscope Software	Zeiss	
Seahorse Wave Desktop	Agilent	
PrimerBank	https://pga.mgh.harvard.edu/primerbank/	

PRIMERS FOR qPCR		
GAPDH	PrimerBank ID: 83641890b1	F: AAGGTGAAGGTCGGAGTCAAC R: GGGGTCATTGATGGCAACAATA
PGC 1α	PrimerBank ID: 116284374c1	F: TCTGAGTCTGTATGGAGTGACAT R: CCAAGTCGTTCACATCTAGTTCA
PGC 1β	PrimerBank ID: 289577089c1	F: GATGCCAGCGACTTTGACTC R: ACCCACGTCATCTTCAGGGA
PRC	PrimerBank ID: 40807451c1	F: CAAGCGCCGTATGGGACTTT R: GGAGGCATCCATGTAGCTCT
NRF 1	PrimerBank ID: 93141038c1	F: AGGAACACGGAGTGACCCAA R: TATGCTCGGTGTAAGTAGCCA
NRF 2	PrimerBank ID: 372620347c1	F: TCAGCGACGGAAAGAGTATGA R: CCACTGGTTTCTGACTGGATGT